A New Discrete Analytic Signal for Reducing Aliasing in the Discrete Wigner-Ville Distribution

John M. O' Toole, *Student Member, IEEE*, Mostefa Mesbah, and Boualem Boashash, *Fellow, IEEE*

***Abstract*—It is not possible to generate an alias-free discrete Wigner–Ville distribution (DWVD) from a discrete analytic signal. This is because the discrete analytic signal must satisfy two mutually exclusive constraints. We present, in this paper, a new discrete analytic signal that improves on the commonly used discrete analytic signal's approximation of these two constraints. Our analysis shows that—relative to the commonly used signal—the proposed signal reduces aliasing in the DWVD by approximately 50%. Furthermore, the proposed signal has a simple implementation and satisfies two important properties, namely, that its real component is equal to the original real signal and that its real and imaginary components are orthogonal.**

***Index Terms*—Analytic signal, antialiasing, discrete Hilbert transforms, discrete Wigner–Ville distribution (DWVD), time–frequency analysis.**

I. Introduction

NEITHER time- nor frequency-domain based methods are suitable for analyzing nonstationary signals. Time-frequency methods, which represent the signal in the joint time–frequency domain, provide appropriate analysis tools—they are able to display the time-varying frequency content which characterize nonstationary signals.

The Wigner–Ville distribution (WVD) is an example of a time–frequency domain representation. The distribution is one of the more widely studied types of time–frequency representations, and is known as the fundamental distribution in the class of quadratic time–frequency distributions [1]. The WVD uses the analytic associate of the real-valued signal, rather than the real-valued signal itself [2]. The WVD is free from cross-term artefacts—present when the real-valued signal is used—between the positive and negative components in the distribution [3].

A. Analytic Signals

We can form the analytic signal $z(t)$, associated with real-valued signal $s(t)$, by eliminating the negative frequency components of $s(t)$[1, p. 13]. In this process, no information is lost as the spectrum of $s(t)$ is (conjugate) symmetrical about the origin for negative and positive frequencies. The spectral definition of the analytic signal implies that $z(t)$ is a complex signal. Apart from its one-sided spectral definition, the analytic signal has two important properties [4]. The first, which we call the recovery property, states that the real component of the analytic signal is equal to the original real-valued signal. Thus, the original signal is recoverable from the analytic signal as $\Re[z(t)] = s(t)$. The second, which we call the orthogonality property, states that the real and imaginary components of the analytic signal are orthogonal. That is, the inner product of the real and imaginary parts is zero, $\langle \Re[z(t)], \Im[z(t)] \rangle = 0$

The discrete WVD (DWVD) requires a discrete analytic signal. (We use the term *discrete analytic signal* to refer to a discrete version of the continuous analytic signal, even though this discrete signal is not an analytic function of a continuous complex variable [4].) Various methods for forming discrete analytic signals exist. We classify these methods as either time-domain [5], [6] or frequency-domain [4], [7] based methods. The most commonly used approach [3], [8]–[10] for generating discrete analytic signals for the DWVD is a frequency-domain method [4]. This method, which can be simply implemented, results in a discrete analytic signal that satisfies the recovery and orthogonality properties.

B. An Alias-Free Discrete Wigner–Ville Distribution

The DWVD is discrete in both the time and frequency directions—a requirement for digital signal processing applications [9]. The DWVD is formed from either a discrete-time signal $z[n]$ or its discrete Fourier transform (DFT) counterpart $Z[k]$. To obtain an alias-free DWVD, the N-point discrete signal must satisfy two constraints [11]. First, $Z[k]$ must be zero at the Nyquist frequency term and for all negative frequencies—that is, $Z[k] = 0$ for $N/2 \leq k \leq N-1$. (The segment $N/2 < k \leq N-1$ represents the negative frequencies and $k = N/2$ represents the Nyquist frequency.) Second, $z[n]$ must be zero for the second half of its time duration—that is, $z[n] = 0$ for $N/2 \leq n \leq N-1$. To satisfy this condition and maintain the integrity of the signal, we replace the N-point signal $z[n]$ with the $2N$-point zero-padded signal $z_c[n]$[5]. Thus, the two (modified) constraints required for an alias-free DWVD are

$$z_c[n] = 0, \quad \text{for } N \leq n \leq 2N-1 \tag{1}$$

$$Z_c[k] = 0, \quad \text{for } N \leq k \leq 2N-1 \tag{2}$$

where $Z_c[k]$ is the DFT of $z_c[n]$. We shall refer to (1) as the *time-constraint* and (2) as the *frequency-constraint*.

Manuscript received August 20, 2007; revised June 22, 2008. First published August 8, 2008; current version published October 15, 2008. The associate editor coordinating the review of this paper and approving it for publication was Dr. Mark J. Coates.

J. M. O'Toole and M. Mesbah are with the Perinatal Research Centre, University of Queensland, Royal Brisbane & Women's Hospital, Herston, QLD 4029, Australia (e-mail: j.otoole@ieee.org; j.otoole@uq.edu.au; m.mesbah@uq.edu.au).

B. Boashash is with the Perinatal Research Centre, University of Queensland, Royal Brisbane & Women's Hospital, Herston, QLD 4029, Australia, and also with the College of Engineering, University of Sharjah, Sharjah, U.A.E. (e-mail: b.boashash@uq.edu.au).

Digital Object Identifier 10.1109/TSP.2008.929325

Unfortunately, the zero-padding procedure used in (1) introduces energy at negative frequencies, thus violating the frequency-constraint of (2). In fact, this requirement for a simultaneous finite-time duration, finite-bandwidth constraint is a theoretical impossibility [12]. Nevertheless, any energy in either of these regions will produce aliasing in the DWVD [11].

C. A New Discrete Analytic Signal

We present, in this article, a new discrete analytic signal based on the commonly used discrete analytic signal [4]. Like the commonly used signal, which we refer to as the *conventional* discrete analytic signal, the proposed signal satisfies the time-constraint of (1) but only approximates the frequency-constraint of (2). We measure this approximation by quantifying the amount of energy in the ideally-zero region in (2). We use this measure to compare the performance of the proposed and conventional discrete analytic signals. In addition, we numerically compare, using a number of signals, the amount of aliasing energy in the DWVD of the two discrete analytic signals.

We found that the proposed signal, relative to the conventional signal, reduces aliasing in the DWVD by approximately one-half. This result agrees with our initial result—that the proposed signal, relative to the conventional signal, better approximates the frequency-constraint of (2). Also, the proposed signal satisfies the recovery and orthogonality properties and can be computed simply using DFTs.

II. Discrete Analytic Signals for the Discrete Wigner-Ville Distribution

A. Discrete Wigner-Ville Distribution

To compute the DWVD of an N-point real-valued discrete signal $s[n]$, we first form the $2N$-point discrete analytic signal $z_{\rm c}[n]$ from $s[n]$. Then, we use $z_{\rm c}[n]$, or its DFT associate $Z_{\rm c}[k]$, to define the DWVD [11] as

$$W[n,k] = \sum_{m=0}^{2N-1} z_{\rm c}[m] z_{\rm c}^*[n-m]\, {\rm e}^{-{\rm j}\pi(m-n/2)k/N} \quad (3)$$

$$= \frac{1}{2N} \sum_{l=0}^{2N-1} Z_{\rm c}[l] Z_{\rm c}^*[k-l]\, {\rm e}^{{\rm j}\pi(l-k/2)n/N}. \quad (4)$$

The signals $z_{\rm c}[n]$ and $Z_{\rm c}[k]$ are periodic in $2N$. We present this particular DWVD definition here as it satisfies more desirable mathematical properties than other DWVD definitions [5], [10], [11]. The implications, however, arising from the choice of analytic signal are the same regardless of the DWVD definition. To generate $z_{\rm c}[n]$ from $s[n]$ involves a number of steps, which we describe in the next subsection.

B. Discrete Analytic Signals

1) Desirable Properties: There is no unique definition for a discrete analytic signal. The discrete definition should, however, conserve as many properties inherent to the continuous analytic signal as possible. Marple [4] proposed that a discrete analytic signal should at least satisfy the recovery and orthogonality properties.

We detail these two properties as follows. For a discrete analytic signal $z[n]$, associated with the N-point real-valued signal $s[n]$, the recovery property is

$$\Re(z[n]) = s[n], \qquad \text{for } 0 \le n \le N-1 \quad (5)$$

and orthogonality property is

$$\sum_{n=0}^{N-1} \Re(z[n])\, \Im(z[n]) = 0. \quad (6)$$

(We shall refer to the discrete analytic signal simply as an analytic signal when the context is clear.)

2) Review: We classify existing methods for forming analytic signals as either time- or frequency-domain based methods. First, we look at two time-domain based methods. One method uses dual quadrature FIR filters to jointly produce the real and imaginary components of $z[n]$, as described in [6]. The resultant analytic signal satisfies the orthogonality property but not the recovery property [4]. The other method forms the analytic signal using the relation $z[n] = s[n] + {\rm j}\mathcal{H}(s[n])$, by approximating the Hilbert transform operation $\mathcal{H}(\cdot)$ with an FIR filter [6]. The resultant analytic signal satisfies the recovery property but not the orthogonality property.

Next, we look at two frequency-domain based procedures. One method forms the analytic signal by setting the negative frequency samples to zero [4]. This method, originally proposed in discrete Hilbert transform form by Čížek [13] and Bonzanigo [14], uses the DFT and inverse DFT (IDFT) to switch between the time and frequency domains. The method, which we shall refer to as the Čížek–Bonzanigo method, satisfies both properties. The other frequency-domain based method [7] is a modified version of the Čížek–Bonzanigo method; it has the additional step of zeroing an extra single value of the continuous spectrum in the negative frequency range. The method satisfies the recovery property but not the orthogonality property.

Comparative to the other methods, the analytic signal produced by the Čížek–Bonzanigo method is particularly attractive for the following reasons:

- its negative frequency samples are exactly zero;
- it preserves the recovery and orthogonality properties;
- it has a simple implementation [4]—no filter design [6] or selection of an arbitrary frequency point [7] is necessary.

The commonly used procedure for obtaining an analytic signal for a DWVD uses the Čížek-Bonzanigo method. The complete procedure, for the N-point real-valued signal $s[n]$, is as follows [3], [8]–[10]:

1) take the DFT of signal $s[n]$ to obtain $S[k]$;
2) let $\widehat{Z}_{\rm c}[k] = \widehat{H}_{\rm c}[k] S[k]$, with $\widehat{H}_{\rm c}[k]$ defined as

$$\widehat{H}_{\rm c}[k] = \begin{cases} 1, & k = 0 \text{ and } k = \frac{N}{2}, \\ 2, & 1 \le k \le \frac{N}{2} - 1, \\ 0, & \frac{N}{2} + 1 \le k \le N-1; \end{cases}$$

3) take the IDFT of $\widehat{Z}_{\rm c}[k]$ to obtain $\hat{z}_{\rm c}[n]$ (of length N);
4) let $z_{\rm c}[n]$ equal $\hat{z}_{\rm c}[n]$ zero-padded to length $2N$; we call $z_{\rm c}[n]$ the *conventional* analytic signal.

The last step ensures that $z_{\rm c}[n]$ satisfies the time-constraint of (1), and therefore not the frequency-constraint of (2). In addition, the Čížek–Bonzanigo method does not zero the Nyquist frequency term, which also violates the frequency-constraint.

III. Proposed Discrete Analytic Signal

The procedure to form the proposed analytic signal $z_{\rm p}[n]$[15], from the N-point real-valued signal $s[n]$, is as follows:

1) zero-pad $s[n]$ to length $2N$; call this $s_{\rm a}[n]$;
2) take the DFT of $s_{\rm a}[n]$ to obtain $S_{\rm a}[k]$;
3) let

$$Z_{\rm a}[k] = H_{\rm a}[k]S_{\rm a}[k] \tag{7}$$

where $H_{\rm a}[k]$ is defined as

$$H_{\rm a}[k] = \begin{cases} 1, & k = 0 \text{ and } k = N, \\ 2, & 1 \le k \le N-1, \\ 0, & N+1 \le k \le 2N-1; \end{cases} \tag{8}$$

4) take the IDFT of $Z_{\rm a}[k]$ to obtain $z_{\rm a}[n]$;
5) and lastly, force the second half of $z_{\rm a}[n]$ to zero

$$z_{\rm p}[n] = \begin{cases} z_{\rm a}[n], & 0 \le n \le N-1, \\ 0, & N \le n \le 2N-1. \end{cases}$$

Steps 2) to 4) implements the Čížek–Bonzanigo method on the zero-padded signal $s_{\rm a}[n]$ [16]. We, therefore, do the zero-padding process before we generate the signal $z_{\rm a}[n]$, unlike the procedure for $z_{\rm c}[n]$, where we do the zero-padding process last. The last step ensures that $z_{\rm p}[n]$ satisfies the time-constraint of (1), although at the expense of the frequency-constraint of (2).

We can easily show that, like the conventional analytic signal, the proposed signal satisfies the recovery and orthogonality properties presented in Section II-B-1).

A. Time-Domain Analysis

The two analytic signals are related to the $2N$-point real-valued signal $s_{\rm a}[n]$ as follows:

$$z_{\rm c}[n] = (s_{\rm a}[n] \circledast h_{\rm c}[n])\, u_{\rm t}[n] \tag{9}$$

$$z_{\rm p}[n] = (s_{\rm a}[n] \circledast h_{\rm a}[n])\, u_{\rm t}[n] \tag{10}$$

where $\circledast$ represents circular convolution. The time-reversed and time-shifted step function $u_{\rm t}[n]$ is defined as $u_{\rm t}[n] = u[N-1-n]$, where $u[n]$ represents the unit step function. The impulse function $h_{\rm a}[n]$ is the IDFT of the frequency-response function $H_{\rm a}[k]$, defined in (8). We can show that this impulse function equates to

$$h_{\rm a}[n] = \begin{cases} \delta[n], & n \text{ even} \\ \frac{1}{N}\cot\left(\frac{\pi n}{2N}\right), & n \text{ odd} \end{cases}$$

where $\delta[n]$ is the Kronecker delta function. The relation between the two convolving functions $h_{\rm c}[n]$ and $h_{\rm a}[n]$ is

$$h_{\rm c}[n] = h_{\rm a}[n] + h_{\rm a}[n+N]. \tag{11}$$

The presence of $u_{\rm t}[n]$ in (9) and (10) guarantees that $z_{\rm c}[n]$ and $z_{\rm p}[n]$ both satisfy the time-constraint.

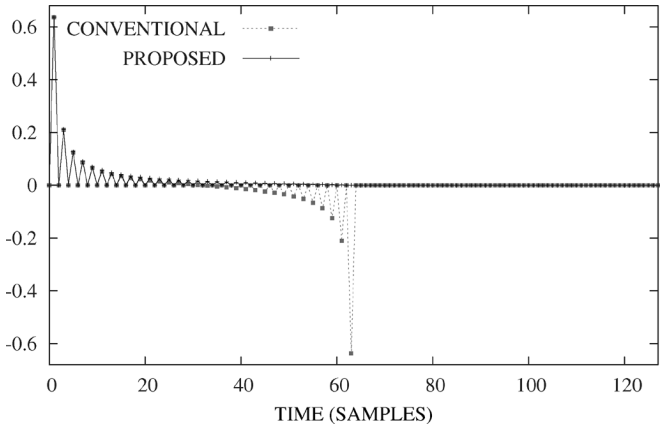

Fig. 1. Imaginary part of the conventional and proposed analytic signals formed from the N-point impulse signal, where $N = 64$.

To highlight the differences between the two analytic signals, we use the N-point impulse signal $s[n] = \delta[n]$ as an example. As both analytic signals preserve the real-valued signal, only the imaginary components for the signals are plotted in Fig. 1. As expected, the imaginary parts of $z_{\rm c}[n]$ and $z_{\rm p}[n]$ are zero for $N \le n \le 2N-1$, because the presence of $u_{\rm t}[n]$ in (9) and (10) guarantee that both signals satisfy the time-constraint. Also, $z_{\rm c}[n]$ has a significant negative component around $n = N-1$, whereas $z_{\rm p}[n]$ does not. The relation in (11) explains this difference.

B. Frequency-Domain Analysis

In the frequency domain, the two analytic signals as a function of $S_{\rm a}[k]$ are

$$Z_{\rm c}[k] = (S_{\rm a}[k]H_{\rm c}[k]) \circledast U_{\rm t}[k] \tag{12}$$

$$Z_{\rm p}[k] = (S_{\rm a}[k]H_{\rm a}[k]) \circledast U_{\rm t}[k] \tag{13}$$

where $S_{\rm a}[k]$ is the DFT of $s_{\rm a}[n]$ and $U_{\rm t}[k]$ is the DFT of $u_{\rm t}[n]$. The frequency-response function $H_{\rm c}[k]$ is

$$H_{\rm c}[k] = \begin{cases} 2H_{\rm a}[k], & k \text{ even} \\ 0, & k \text{ odd} \end{cases} \tag{14}$$

with $H_{\rm a}[k]$ defined in (8). Because of the convolution with $U_{\rm t}[k]$ in (12) and (13), neither $Z_{\rm c}[k]$ nor $Z_{\rm p}[k]$ satisfy the frequency-constraint.

To illustrate the difference between the two analytic signals' spectra, we use the impulse signal once more. These results are displayed in Fig. 2. For this signal $S_{\rm a}[k] = 1$ for all values of k. Neither signal satisfies the frequency-constraint. The conventional analytic signal's approximation—comparative to the proposed analytic signal—of the frequency-constraint, however, is marred by significant oscillation between the odd and even values of k. The oscillatory nature of $H_{\rm c}[k]$ causes this behavior, as described by (14).

IV. Performance of Proposed Analytic Signal

In this section, we examine the performance of the proposed analytic signal—relative to the conventional analytic signal—at approximating the frequency-constraint of (2).

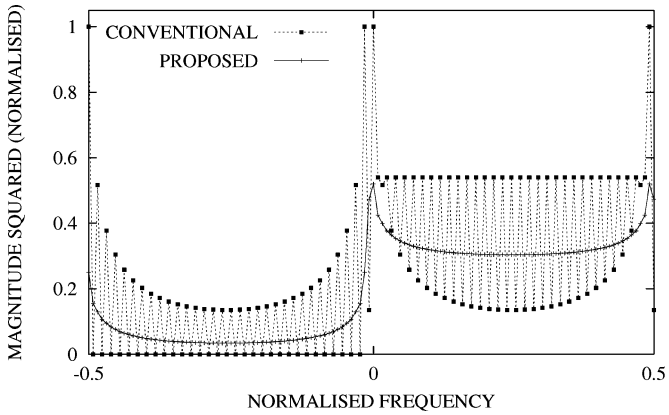

Fig. 2. Discrete spectra of the two analytic signals formed from the test impulse signal.

A. Relative Performance

We use the signals' spectral energy, at the Nyquist and negative frequencies, as a relative performance measure. The following proposition describes this measure.

Proposition 1: The spectral energy relation of $Z_{\rm p}[k]$ and $Z_{\rm c}[k]$, at Nyquist and negative frequencies, is

$$\sum_{k=N}^{2N-1} |Z_{\rm p}[k]|^2 = \frac{1}{2}\sum_{k=N}^{2N-1} |Z_{\rm c}[k]|^2 + \frac{1}{2}\left(|Z_{\rm p}[N]|^2 - \left|\widehat{Z}[0]\right|^2 - C\right) \quad (15)$$

where $\widehat{Z}[k] = Z_{\rm a}[k] - Z_{\rm p}[k]$, with $Z_{\rm a}[k]$ defined in (7), and

$$C = \begin{cases} 0, & N \text{ even} \\ 2\left|\widehat{Z}[N]\right|^2, & N \text{ odd.} \end{cases}$$

Proof: See the Appendix. □

From (15), we see that the energy relation between $Z_{\rm p}[k]$ and $Z_{\rm c}[k]$ is dependent on the value of $Z_{\rm a}[k]$ and $Z_{\rm p}[k]$ at $k = 0$ and $k = N$. If the second term in the right-hand side of (15) is small, relative to the first term, then we can rewrite (15) as

$$\sum_{k=N}^{2N-1} |Z_{\rm p}[k]|^2 \approx \frac{1}{2}\sum_{k=N}^{2N-1} |Z_{\rm c}[k]|^2 . \quad (16)$$

This equation states that the spectral energy for $Z_{\rm p}[k]$ is approximately half of the spectral energy for $Z_{\rm c}[k]$ in the specified range. We numerically verify this approximation in the next subsection using a number of test signals.

B. Numerical Examples

This section provides examples to confirm the approximation in (16). To start, we define the ratio

$$\eta = \frac{\sum_{k=N}^{2N-1} |Z_{\rm p}[k]|^2}{\sum_{k=N}^{2N-1} |Z_{\rm c}[k]|^2}.$$

Next, we compute this ratio with six different signal types: an impulse function, a step function, a sinusoidal signal, a nonlinear frequency modulated signal (NLFM) signal, white Gaussian noise (WGN), and a real-world signal. This last signal is an electroencephalogram (EEG) recording from a newborn baby. The length N for each signal was arbitrarily set to even values between 14 and 2048; 1 was added to this value to obtain N odd.

TABLE I
PERFORMANCE RATIO MEASURES COMPARING THE PROPOSED WITH THE CONVENTIONAL ANALYTIC SIGNAL

Signal Type	η (N even)	η (N odd)
Impulse	0.5078	0.4711
Step	0.4137	0.4136
Sinusoid	0.4595	0.5709
NLFM	0.5055	0.4999
WGN[a]	0.5883 (0.0976)	0.5319 (0.0983)
EEG[b]	0.4184 (0.0671)	0.4155 (0.0650)

[a] 1000 realisations used. [b] 1000 epochs used.
[a,b] Values are in the form, mean (standard deviation).

The results, in Table I, for most of the test signals confirm the approximation stated in (16). The exceptions to this include the WGN realizations, where the mean ratio value is < 0.6, and the sinusoidal signal when N is odd, where the ratio value is also < 0.6.

In addition, we plot, in Fig. 3, the spectra of the conventional and proposed analytic signals using two of the tests signals: the sinusoidal signal with $N = 14$, and an EEG epoch with $N = 99$. Note, from Figs. 3 and 2, that the amount of energy in the negative spectral region is signal dependent, but the ratio η comparing the analytic signals remains approximately the same.

V. Reduced Aliased DWVD

This section compares the performance of the analytic signals by their contribution to aliasing in the DWVD.

A. Aliasing in the DWVD of $z_{\rm p}[n]$

To begin, we recall how we quantify aliasing in the discrete-time domain. Consider a continuous-time signal $y(t)$, bandlimited in the frequency-domain to the region $|f| < 1/2T$. We sample $y(t)$, with sampling period T, to obtain the discrete-time signal $y[n]$. This signal $y[n]$ is alias free because the periodic copies in the frequency domain for $y[n]$ do not overlap. Now consider another discrete signal $y_1[n]$, obtained by sampling $y(t)$ with sampling period $T_1 = 2T$. This discrete signal $y_1[n]$ is aliased because the periodic copies in the frequency-domain do overlap. If we know the spectral content for $y(t)$, then we are able to measure the spectral periodic overlap for $y_1[n]$, and are therefore able to quantify the aliasing in $y_1[n]$. Similarly, to evaluate aliasing in the DWVD, we measure spectral content in a specific region of the doppler-frequency domain.

The asymmetrical doppler-frequency function of the analytic signal $Z[k]$, defined as

$$\mathcal{K}[l,k] = Z[l]Z^*[k-l]$$

is used to form the DWVD in (4). If we assume that $Z[k]$ satisfies the frequency-constraint of (2), then the nonzero content (or energy) in $\mathcal{K}[l,k]$ is contained within a specific region. Any energy, however, outside this region results in aliasing in the DWVD. We refer to this undesirable phenomenon as *spectral-leakage*.

As $Z_{\rm c}[k]$ does not satisfy the frequency-constraint, its doppler-frequency function $\mathcal{K}_{\rm c}[l,k]$ contains spectral-leakage.

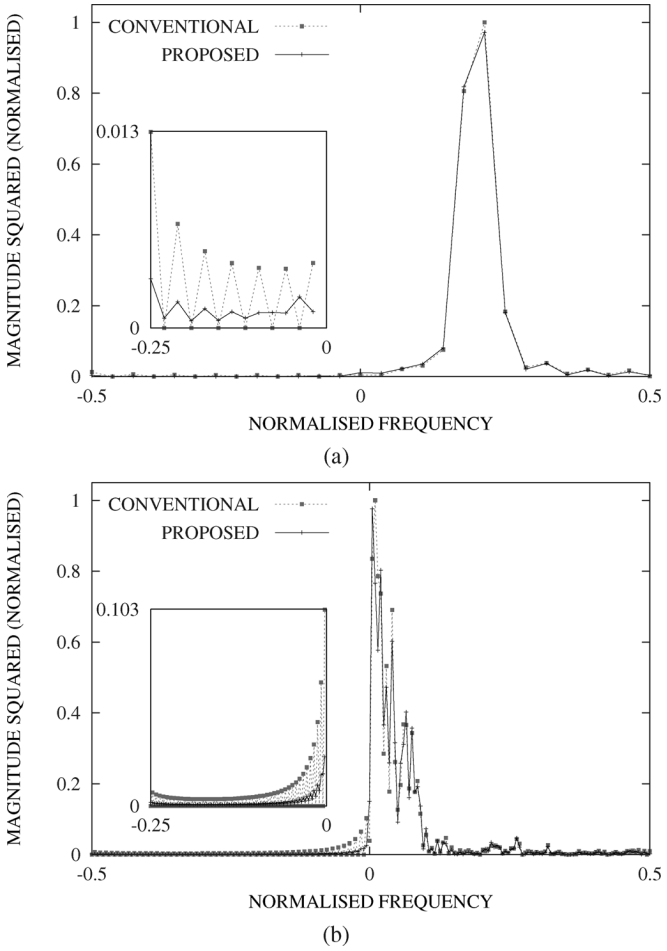

Fig. 3. Discrete spectra comparing the two analytic signals for two test signals: (a) a sinusoidal signal, and (b) an EEG epoch. The inset plots show a portion of the negative frequency axis with a reduced magnitude range.

This is true also for the doppler-frequency function of $Z_{\mathrm{p}}[k]$, $\mathcal{K}_{\mathrm{p}}[l,k]$. We quantify this spectral-leakage by summing the squared error over this region, where the ideal here is zero. Accordingly, to asses the relative merit of the proposed analytic signal, we use the ratio squared error measure

$$\mu = \frac{\alpha(\mathcal{K}_{\mathrm{p}})}{\alpha(\mathcal{K}_{\mathrm{c}})}$$

where $\alpha(\mathcal{K})$ is a measure of the two-dimensional spectral-leakage for $\mathcal{K}[l,k]$, defined as

$$\alpha(\mathcal{K}) = \sum_{k=0}^{2N-1}\sum_{l=N}^{2N-1} |\mathcal{K}[l,k]|^2 + \sum_{k=N}^{2N-1}\sum_{l=0}^{k-N} |\mathcal{K}[l,k]|^2 + \sum_{k=0}^{N}\sum_{l=k+1}^{N} |\mathcal{K}[l,k]|^2 .$$

As the function $\mathcal{K}[l,k]$ is quadratic in $Z[k]$, cross-terms between the positive and negatives frequencies will be present in the resultant DWVD. These cross-terms are part of the spectral-leakage in the doppler-frequency function, and are therefore incorporated into the $\alpha(\mathcal{K})$ measure. We consider these cross-terms as aliasing as they would not be present if the frequency-constraint was satisfied.

TABLE II
PERFORMANCE RATIO MEASURES COMPARING ALIASING IN THE DWVD OF THE PROPOSED ANALYTIC SIGNAL WITH THE DWVD OF THE CONVENTIONAL ANALYTIC SIGNAL

Signal Type	μ (N even)	μ (N odd)
Impulse	0.4034	0.3750
Step	0.4101	0.4099
Sinusoid	0.4545	0.5600
NLFM	0.5055	0.4998
WGN[a]	0.5840 (0.0984)	0.5371 (0.0996)
EEG[b]	0.4140 (0.0723)	0.4112 (0.0705)

[a] 1000 realisations used. [b] 1000 epochs used.
[a,b] Values are in the form, mean (standard deviation).

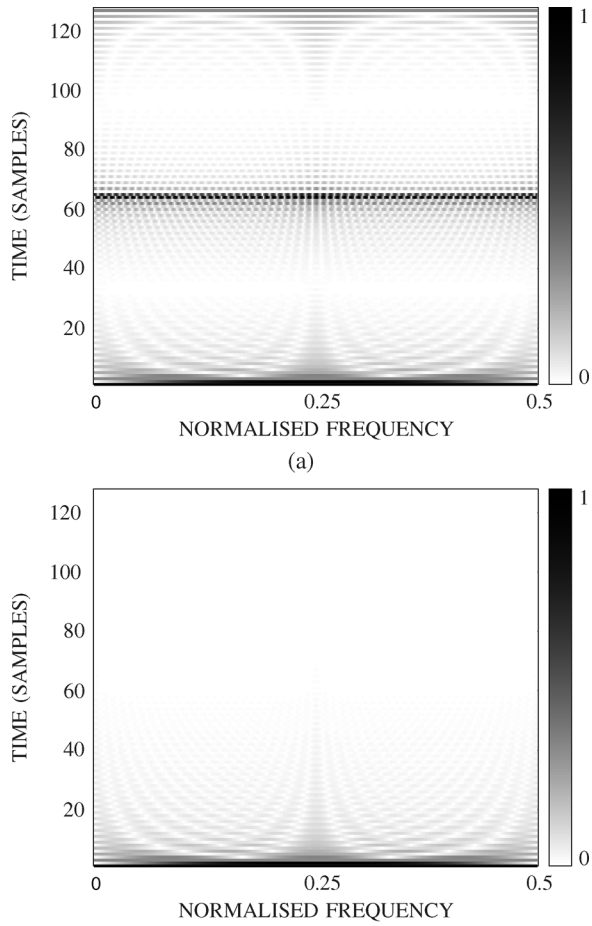

Fig. 4. DWVDs of the two analytic signals using the impulse test signal $\delta[n]$: absolute value of the DWVD for the (a) conventional analytic signal, and (b) proposed analytic signal. Both DWVDs are normalized.

B. Numerical Examples

We present the results in Table II for the same set of example signals used in Section IV-B. The results for μ are not equal to η because the doppler-frequency function $\mathcal{K}[l,k]$ is quadratic in the signal $Z[k]$. We see from the results, however, that μ approximates η for all test signals apart from the impulse signal, where μ is less than η. From these results we infer that the amount of spectral-leakage for $\mathcal{K}_{\mathrm{p}}[l,k]$ is approximately half of the spectral-leakage for $\mathcal{K}_{\mathrm{c}}[l,k]$. Hence, the amount of aliasing present

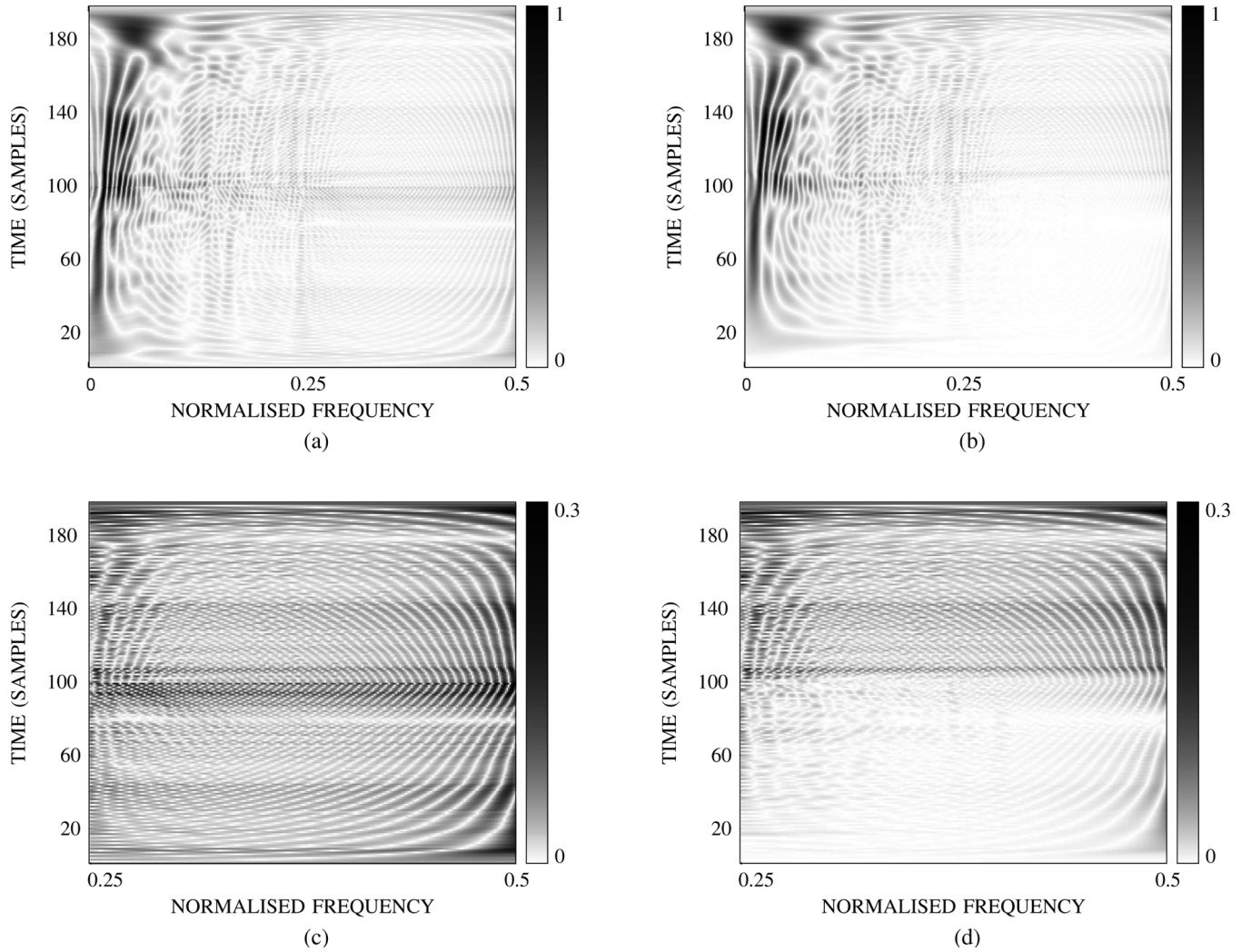

Fig. 5. DWVDs of the two analytic signals using an EEG epoch: absolute value of the DWVD for the (a) conventional analytic signal, and (b) proposed analytic signal. To highlight the differences between the distributions, (c) and (d) display a portion of the distribution where, for this particular signal, we expect little energy. The plot in (c) is one-half of the distribution in (a); likewise, the plot in (d) is one-half of the distribution in (b). Both DWVDs are normalized.

in the DWVD of $z_{\mathrm{p}}[n]$ is approximately half of the aliasing present in the DWVD of $z_{\mathrm{c}}[n]$.

To show some examples of this reduced aliasing, we plot the DWVDs of the two analytic signals using two different signals from the test set—namely, the impulse signal and an EEG epoch. Fig. 4 shows the two DWVDs of the impulse signal. For this signal, the energy in the DWVD should, ideally, be concentrated around the time sample $n = 0$, as $\delta[n] = 0$ for $n > 0$. Fig. 4 shows that the DWVD of the proposed analytic signal better approximates this ideal compared with the DWVD of the conventional analytic signal.

In Fig. 5 we show the two DWVDs using the EEG epoch. We previously plotted the spectra of the two analytic signals for this EEG epoch in Fig. 3(b). From this frequency-domain plot, we can see that very little relative energy is present above the normalized frequency value of 0.25. Thus, we expect little energy in the DWVD above the frequency value 0.25. Accordingly, from Fig. 5, we see that the DWVD of the proposed signal has less energy in this region compared with that for the DWVD of the conventional analytic signal.

VI. Conclusion

The failure of a discrete analytic signal to satisfy both a finite-time and finite-frequency bandwidth constraint causes aliasing in the DWVD. We presented, in this article, a new discrete analytic signal which, compared with the conventional discrete analytic signal, better approximates these constraints and consequently reduces aliasing in the DWVD. We showed that the DWVD of our proposed analytic signal has approximately 50% less aliasing than that for the DWVD of the conventional analytic signal. The proposed signal retains two useful attributes of the conventional signal: it satisfies the recovery and orthogonality properties and has a simple implementation using DFTs.

Matlab and Octave code to generate the discrete analytic signals is available online at http://espace.library.uq.edu.au/view/UQ:151384.

Appendix
Proof of Proposition 1

We derive the relation, for the negative spectral energy, between the proposed and conventional analytic signals. To do so,

we decompose the energy of $Z_{\rm p}[k]$ for $N \le k \le 2N-1$ as follows:

$$\sum_{k=N}^{2N-1} |Z_{\rm p}[k]|^2 = |Z_{\rm p}[N]|^2 + \sum_{k=\lfloor N/2\rfloor+1}^{N-1} |Z_{\rm p}[2k]|^2 + \sum_{k=\lceil N/2\rceil}^{N-1} |Z_{\rm p}[2k+1]|^2 \quad (17)$$

where the function $\lfloor x \rfloor$ returns an integer smaller than or equal to x, and the function $\lceil x \rceil$ returns an integer larger than or equal to x. We examine each part of the preceding decomposition separately.

Case for k Odd: First, we write $U_{\rm t}[k]$, which is the DFT of $u_{\rm t}[n]$, as

$$U_{\rm t}[k] = \begin{cases} N\delta[k], & k \text{ even} \\ 1 - {\rm j}\cot\left(\frac{\pi k}{2N}\right), & k \text{ odd.} \end{cases} \quad (18)$$

Next, we consider the energy at negative frequencies for $Z_{\rm c}[k]$. From (12) and (14), we express $Z_{\rm c}[k]$ as

$$Z_{\rm c}[k] = \frac{1}{N}\sum_{l=0}^{N-1} S_{\rm a}[2l]H_{\rm a}[2l]U_{\rm t}[k-2l].$$

If we use (18) in the preceding equation, then we can write $Z_{\rm c}[k]$ for even-odd k values as

$$Z_{\rm c}[2k] = S_{\rm a}[2k]H_{\rm a}[2k] \quad (19)$$

$$Z_{\rm c}[2k+1] = \frac{1}{N}\sum_{l=0}^{N-1} S_{\rm a}[2l]H_{\rm a}[2l]U_{\rm t}[2k+1-2l]. \quad (20)$$

The even k terms for $Z_{\rm c}[k]$ do not contribute to the negative spectral energy because, from (8), $H_{\rm a}[2k] = 0$ for $2k > N$. Thus, the energy in the negative spectral region is solely caused by the odd k terms in $Z_{\rm c}[k]$,

$$\sum_{k=N+1}^{2N-1} |Z_{\rm c}[k]|^2 = \sum_{k=\lceil N/2\rceil}^{N-1} |Z_{\rm c}[2k+1]|^2. \quad (21)$$

Last, we consider the energy at negative frequencies for $Z_{\rm p}[k]$. By combining (13) and (18), $Z_{\rm p}[k]$ for odd k values is

$$Z_{\rm p}[2k+1] = \frac{1}{2}S_{\rm a}[2k+1]H_{\rm a}[2k+1] + \frac{1}{2N}\sum_{l=0}^{N-1} S_{\rm a}[2l]H_{\rm a}[2l]U_{\rm t}[2k+1-2l]. \quad (22)$$

Thus, relating (22) with (20) and (7), we get

$$Z_{\rm p}[2k+1] = \frac{1}{2}\left(Z_{\rm a}[2k+1] + Z_{\rm c}[2k+1]\right). \quad (23)$$

From (8), we know that $Z_{\rm a}[k] = 0$ for $k > N$; therefore, (23) reduces to $Z_{\rm p}[2k+1] = Z_{\rm c}[2k+1]/2$ for $(2k+1) > N$. If we combine this relation with (21), then we get the negative spectral energy relation,

$$\sum_{k=\lceil N/2\rceil}^{N-1} |Z_{\rm p}[2k+1]|^2 = \frac{1}{4}\sum_{k=N+1}^{2N-1} |Z_{\rm c}[k]|^2. \quad (24)$$

Case for k Even: We start by introducing a new signal $\hat{z}[n]$, defined as

$$\hat{z}[n] = \begin{cases} 0, & 0 \le n \le N-1 \\ z_{\rm a}[n], & N \le n \le 2N-1. \end{cases} \quad (25)$$

The signal $\hat{z}[n]$ is purely imaginary because the real part of $z_{\rm a}[n]$ is zero for $N \le n \le 2N-1$. We can also express $\hat{z}[n]$ as $\hat{z}[n] = z_{\rm a}[n] - z_{\rm p}[n]$ for all values of n. In the frequency domain, this equates to

$$\widehat{Z}[k] = Z_{\rm a}[k] - Z_{\rm p}[k]. \quad (26)$$

where $\widehat{Z}[k]$ represents the DFT of $\hat{z}[n]$. We now introduce some properties of $\widehat{Z}[k]$.

We can show easily, because of the form of $\hat{z}[n]$ in (25), that

$$\sum_{k=0}^{N-1} \left|\widehat{Z}[2k]\right|^2 = \sum_{k=0}^{N-1} \left|\widehat{Z}[2k+1]\right|^2. \quad (27)$$

Also, because $\hat{z}[n]$ is purely imaginary then following symmetry holds:

$$\widehat{Z}[2N-k] = -\widehat{Z}^*[k]. \quad (28)$$

We express the spectral energy for $\widehat{Z}[2k]$, using the symmetrical relation in (28), as

$$\sum_{k=0}^{N-1} \left|\widehat{Z}[2k]\right|^2 = \left|\widehat{Z}[0]\right|^2 + 2\sum_{k=\lfloor N/2\rfloor+1}^{N-1} \left|\widehat{Z}[2k]\right|^2 + A. \quad (29)$$

where $A = |\widehat{Z}[N]|^2$ when N is even and $A = 0$ when N is odd.

Similarly, the spectral energy at k odd values of $\widehat{Z}[k]$ is

$$\sum_{k=0}^{N-1} \left|\widehat{Z}[2k+1]\right|^2 = 2\sum_{k=\lceil N/2\rceil}^{N-1} \left|\widehat{Z}[2k+1]\right|^2 + B. \quad (30)$$

where $B = 0$ when N is even and $B = |\widehat{Z}[N]|^2$ when N is odd. This concludes the segment on the properties of $\widehat{Z}[k]$.

If we substitute (30) and (29) into (27), then we obtain:

$$\sum_{k=\lfloor N/2\rfloor+1}^{N-1} \left|\widehat{Z}[2k]\right|^2 = \sum_{k=\lceil N/2\rceil}^{N-1} \left|\widehat{Z}[2k+1]\right|^2 - \frac{1}{2}\left[\left|\widehat{Z}[0]\right|^2 + A - B\right].$$

Then we substitute (24), and the relation $\widehat{Z}[k] = -Z_{\rm p}[k]$ for $k > N$, into the preceding equation to obtain

$$\sum_{k=\lfloor N/2\rfloor+1}^{N-1} |Z_{\rm p}[2k]|^2 = \frac{1}{4}\sum_{k=N+1}^{2N-1} |Z_{\rm c}[k]|^2 - \frac{1}{2}\left[\left|\widehat{Z}[0]\right|^2 + A - B\right]. \quad (31)$$

Nyquist Frequency Terms: The Nyquist term $Z_{\rm a}[N]$ is a real number, because of the definition of $Z_{\rm a}[k]$ in (7); the Nyquist term $\widehat{Z}[N]$ is an imaginary number, because $\hat{z}[n]$ is purely imaginary. Thus, we rewrite (26) as

$$|Z_{\rm p}[N]|^2 = |Z_{\rm a}[N]|^2 + \left|\widehat{Z}[N]\right|^2. \quad (32)$$

The remaining relations depend on the parity of N.

Case for N Even: We know, from (19) and (7), that when N is even, $Z_{\rm c}[N] = Z_{\rm a}[N]$. When we combine this with (32) we get

$$|Z_{\rm p}[N]|^2 = |Z_{\rm c}[N]|^2 + \left|\widehat{Z}[N]\right|^2. \tag{33}$$

Case for N Odd: We know, from (23), that when N is odd, $Z_{\rm c}[N] = 2Z_{\rm p}[N] - Z_{\rm a}[N]$. When we combine this with (26) we get $|Z_{\rm c}[N]|^2 = |Z_{\rm a}[N]|^2 + 4|\widehat{Z}[N]|^2$. If we substitute this equation into (32), then we get the relation

$$|Z_{\rm p}[N]|^2 = |Z_{\rm c}[N]|^2 - 3\left|\widehat{Z}[N]\right|^2. \tag{34}$$

Finally, we are able to assemble the three parts of the decomposition in (17). If we combine the relation for k even in (31) with the relation for k odd in (24), and add the Nyquist frequency relations in (33) and (34), then we get the following:

$$\sum_{k=N}^{2N-1} |Z_{\rm p}[k]|^2 = \frac{1}{2}\sum_{k=N}^{2N-1} |Z_{\rm c}[k]|^2 + \frac{1}{2}\left(|Z_{\rm p}[N]|^2 - \left|\widehat{Z}[0]\right|^2 - C\right)$$

where $C = 2|\widehat{Z}[N]|^2$ when N is odd and $C = 0$ when N is even. This concludes the proof.

REFERENCES

[1] B. Boashash, "Part I: Introduction to the concepts of TFSAP," in *Time–Frequency Signal Analysis and Processing: A Comprehensive Reference*, B. Boashash, Ed. Oxford, U.K.: Elsevier, 2003, ch. 1–3, pp. 3–76.

[2] J. Ville, "Théorie et applications de la notion de signal analytique," (in French) Transl.: English translation: I. Selin, "Theory and applications of the notion of complex signal", Rand Corp. Rep. T-92 (Santa Monica, CA, Aug. 1958) *Cables Et Transmissions*, vol. 2A, no. 1, pp. 61–74, 1948.

[3] B. Boashash, "Note on the use of the Wigner distribution for time–frequency signal analysis," *IEEE Trans. Acoust., Speech, Signal Process.*, vol. 36, no. 9, pp. 1518–1521, Sep. 1988.

[4] S. L. Marple Jr., "Computing the discrete-time 'analytic' signal via FFT," *IEEE Trans. Signal Process.*, vol. 47, no. 9, pp. 2600–2603, Sep. 1999.

[5] T. Claasen and W. Mecklenbräuker, "The Wigner distribution—A tool for time–frequency signal analysis. Part II: Discrete-time signals," *Philips J. Res.*, vol. 35, pp. 276–350, 1980.

[6] A. Reilly, G. Frazer, and B. Boashash, "Analytic signal generation-tips and traps," *IEEE Trans. Signal Process.*, vol. 42, no. 11, pp. 3241–3245, Nov. 1994.

[7] M. Elfataoui and G. Mirchandani, "A frequency domain method for generation of discrete-time analytic signals," *IEEE Trans. Signal Process.*, vol. 54, no. 9, pp. 3343–3352, Sep. 2006.

[8] F. Peyrin, Y. Zhu, and R. Goutte, "A note on the use of analytic signal in the pseudo Wigner distribution," in *Proc. IEEE Int. Symp. Circuits Systems,*, Portland, OR, May 8–11, 1989, vol. 2, pp. 1260–1263.

[9] B. Boashash and G. R. Putland, *Computation of Discrete Quadratic TFDs*, B. Boashash, Ed. Oxford, U.K.: Elsevier, 2003, ch. 6, pp. 268–278.

[10] J. O' Toole, M. Mesbah, and B. Boashash, "A discrete time and frequency Wigner–Ville distribution: Properties and implementation," in *Proc. Int. Conf. Digital Signal Process. Comm. Syst.*, Noosa Heads, Australia, Dec. 19–21, 2005, vol. CD-ROM.

[11] F. Peyrin and R. Prost, "A unified definition for the discrete-time, discrete-frequency, and discrete-time/frequency Wigner distributions," *IEEE Trans. Acoust., Speech, Signal Process.*, vol. ASSP-34, no. 4, pp. 858–867, Aug. 1986.

[12] D. Slepian, "On bandwidth," *Proc. IEEE*, vol. 64, no. 3, pp. 292–300, Mar. 1976.

[13] V.Čížek, "Discrete Hilbert transform," *IEEE Trans. Audio Electroacoust.*, vol. AE-18, no. 4, pp. 340–343, Dec. 1970.

[14] F. Bonzanigo, "A note on 'discrete Hilbert transform'," *IEEE Trans. Audio Electroacoust.*, vol. AE-20, no. 1, pp. 99–100, Mar. 1972.

[15] J. M. O' Toole, M. Mesbah, and B. Boashash, "A new discrete-time analytic signal for reducing aliasing in discrete time–frequency distributions," in *Proc. 15th Eur. Signal Process. Conf. (EUSIPCO)*, Poznań, Poland, Sep. 3–7, 2007, pp. 591–595.

[16] J. M. O' Toole, M. Mesbah, and B. Boashash, "A computationally efficient implementation of quadratic time–frequency distributions," in *Proc. Int. Sym. Signal Process. Its Applications (ISSPA)*, Sharjah, United Arab Emirates, Feb. 12–15, 2007, vol. I, pp. 290–293.

John M. O' Toole (S'07) received the B.E. and M.Eng.Sc. degrees from the University College Dublin, Ireland, in 1997 and 2000, respectively. He is currently working towards the Ph.D. degree at the University of Queensland, Australia.

From 1997 to 1998, he worked as a Research Assistant in the Microwave Research Group at the University College Dublin. He moved to Australia in 2001 and worked as a consultant engineer in control systems from 2001 to 2003. Following this, he worked as a Research Assistant in the Signal Processing Research Centre at the Queensland University of Technology, Australia, from 2003 to 2005. His research interests include time–frequency signal analysis, discrete-time signal processing, efficient algorithm design, and biosignal analysis.

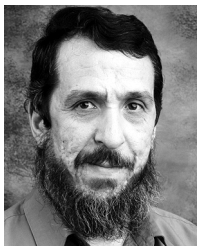

Mostefa Mesbah received the M.S. and Ph.D. degrees in electrical engineering from the University of Colorado, Boulder, in the area of automatic control systems in 1987 and 1992, respectively.

He is currently a Senior Research Fellow at the Perinatal Research Centre, the University of Queensland, Queensland, Australia, supervising a number of Ph.D. students and leading a number of biomedical signal processing projects dealing with the automatic characterization and classification of newborn EEG abnormalities and fetal movement monitoring. His research interests include biomedical signal processing, nonstationary signal processing, sensor fusion, and signal detection and classification.

Boualem Boashash (F'99) received the Diplome d'ingenieur-Physique-Electronique from ICIP University, Lyon, France, in 1978 and the M.S. and Ph.D. (Docteur-Ingenieur) degrees from the Institut National Polytechnique de Grenoble, France, in 1979 and 1982, respectively.

In 1979, he joined Elf-Aquitaine Geophysical Research Centre, Pau, France. In May 1982, he joined the Institut National des Sciences Applique'es de Lyon, France. In 1984, he joined the Electrical Engineering Department of the University of Queensland, Australia, as Lecturer. In 1990, he joined Bond University, Graduate School of Science and Technology, as Professor of electronics. In 1991, he joined Queensland University of Technology as the foundation Professor of signal processing and Director of the Signal Processing Research Centre. Currently, he holds the positions of Dean of the College of Engineering at the University of Sharjah, United Arab Emirates, and Adjunct Professor at the School of Medicine, University of Queensland, Australia. His research interests are time–frequency signal analysis, spectral estimation, signal detection and classification, and higher-order spectra.

Prof. Boashash is Fellow of IE Australia and Fellow of the IREE.